Revista Ciencia e Ingeniería Neogranadina 2025 julio - diciembre Vol. 35(2) ISSN: 0124-8170 · e-ISSN: 1909-7735 ■ pp. 177-188

Editorial Neogranadina

DOI: https://doi.org/10.18359/rcin.7965

Application of Turbulence Models for Calculating the Erosion-Corrosion Rate in N80 Steel with CrSiN Coating*

José Julián Villate Corredor[a] ■ Diego Fernando Gualdron Alfonso[b] ■ Astrid Paola Rodríguez Baquero[c] ■ Jorge Andrés Sarmiento Rojas[d] ■ Carlos Andrés Caro Camargo[e]

Abstract: Corrosion in pipelines poses major operational challenges in industrial facilities worldwide, often resulting in human casualties, service disruptions, and significant environmental and economic impacts. This study aimed to determine the corrosion rate of N80 steel coated with a CrSiN layer by combining experimental techniques with hydrodynamic simulations. The corrosion rate of API-5CT-N80 steel, coated with CrSiN and exposed to an aggressive fluid, was measured using the Electrochemical Resistance (ECR) technique. In parallel, hydrodynamic modeling was conducted with OpenFOAM software, applying a RANS-type approach, a realizable k-ε turbulence model, and the Navier–Stokes equations. From this, an expression was derived to estimate the corrosion rate of the steel as a function of flow velocity, temperature, particle size, and fractional volume. The results indicate that the corrosion rate is strongly influenced by system rotation speed in the presence of small- and medium-sized solid particles. However, this relationship does not hold for flows containing larger particles, where the increase in particle mass reduces their velocity and, consequently, their impact energy.

Keywords: Corrosion Rate; Hydrodynamic Modeling; ECR

* Research article.

a Doctor in Engineering and Materials Science.Universidad Pedagógica y Tecnológica de Colombia, Tunja, Colombia.
Email: jose.villate@uptc.edu.co; ORCID: https://orcid.org/0000-0001-5072-2034

b Magíster in Construction Project Management. Universidad Pedagógica y Tecnológica de Colombia, Tunja, Colombia.
Email: diego.gualdron@uptc.edu.co; ORCID: https://orcid.org/0000-0002-1086-4801

c Magíster in Project Managemet. Universidad Pedagógica y Tecnológica de Colombia, Tujna, Colombia.
Email: Astrid.rodriguez01@uptc.edu.co; ORCID: https://orcid.org/0009-0009-2335-6900

d Doctor in Project Management. Universidad Pedagógica y Tecnológica de Colombia, Tunja, Colombia.
Email: jorge.sarmiento02@uptc.edu.co ; ORCID: https://orcid.org/0000-0002-4230-3304

e Doctor in Civil Engineering (Hydrology). Universidad Pedagógica y Tecnológica de Colombia, Tunja, Colombia.
Email: carlos.caro04@uptc.edu.co; ORCID: https://orcid.org/0000-0001-5568-1219

Recibido: 19/05/2025 **Aceptado:** 30/08/2025 **Disponible en línea:** 22/10/2025

Cómo citar: J. J. Villate Corredor, D. F. Gualdron Alfonso, A. P. Rodríguez Baquero, J. A. Sarmiento Rojas, y C. A. Caro Camargo, «Application of Turbulence Models for Calculating the Erosion-Corrosion Rate in N80 Steel with CrSiN Coating», Cien.Ing.Neogranadina, vol. 35, n.º 2, pp. 177–188, oct. 2025.

Aplicación de modelos de turbulencia para el cálculo de la tasa de erosión-corrosión en acero N80 con recubrimiento de CrSiN

Resumen: La corrosión en tuberías genera importantes problemas operativos en instalaciones industriales de todo el mundo, provocando víctimas humanas, interrupciones del servicio y considerables consecuencias medioambientales y económicas. Este estudio tenía como objetivo establecer la velocidad de corrosión en acero N80 recubierto con CrSiN, empleando tanto técnicas experimentales como simulaciones hidrodinámicas. La velocidad de corrosión del acero API-5CT-N80, recubierto con CrSiN y expuesto a un fluido agresivo, se determinó mediante la técnica de Resistencia Electroquímica (ECR). Simultáneamente, se realizó un modelado hidrodinámico utilizando el software OpenFOAM, aplicando un modelo de tipo RANS, un modelo de turbulencia k-ε realizable y las ecuaciones de Navier-Stokes. Como resultado, se derivó una expresión para determinar la velocidad de corrosión del acero en función de la velocidad de flujo, la temperatura, el tamaño de partícula y el volumen fraccionario. Los resultados indican que la velocidad de corrosión está influida por la velocidad de rotación del sistema cuando se trata de partículas sólidas de tamaño pequeño y mediano. Sin embargo, esta relación no se mantiene para los flujos que contienen partículas de mayor tamaño, en los que el aumento del peso de las partículas provoca una reducción de su velocidad y, en consecuencia, una disminución de la energía de impacto.

Palabras clave: velocidad de corrosión; modelación hidrodinámica; ECR

Aplicação de modelos de turbulência para o cálculo da taxa de erosão-corrosão em aço N80 com revestimento de CrSiN

Resumo: A corrosão em tubulações causa sérios problemas operacionais em instalações industriais em todo o mundo, resultando em vítimas humanas, interrupções de serviço e consideráveis impactos ambientais e econômicos. Este estudo teve como objetivo determinar a velocidade de corrosão em aço N80 revestido com CrSiN, utilizando tanto técnicas experimentais quanto simulações hidrodinâmicas. A taxa de corrosão do aço API-5CT-N80 revestido com CrSiN e exposto a um fluido agressivo foi determinada por meio da técnica de Resistência Eletroquímica (ECR). Simultaneamente, foi realizado um modelamento hidrodinâmico utilizando o software OpenFOAM, aplicando um modelo do tipo RANS, um modelo de turbulência k-ε realizável e as equações de Navier-Stokes. Como resultado, foi derivada uma expressão para determinar a velocidade de corrosão do aço em função da velocidade de fluxo, temperatura, tamanho das partículas e fração volumétrica. Os resultados indicam que a velocidade de corrosão é influenciada pela velocidade de rotação do sistema quando se trata de partículas sólidas de tamanho pequeno e médio. No entanto, essa relação não se mantém em fluxos que contêm partículas de maior tamanho, nas quais o aumento do peso das partículas provoca uma redução em sua velocidade e, consequentemente, uma diminuição na energia de impacto.

Palavras-chave: velocidade de corrosão; modelagem hidrodinâmica; ECR

Introduction

The evolution of industrial facilities has enhanced hydrocarbon production technologies, which in turn has created severe operating conditions for pipelines due to the influence of variables such as temperature, pressure, load, and flow velocity [1]. Combined with the need to transport multiphase flows containing entrained solids, these conditions promote the occurrence of both corrosive and erosive phenomena [2]. Such factors lead to pipeline failures caused by material loss [3], which are directly associated with operational problems in industrial facilities worldwide [4], [5].

Hydrocarbon production involves the extraction of large quantities of water [6], along with sands [7], organic acids, and salts [8], [9], typically transported through carbon steel pipes [8], [10]. Although carbon steel is highly susceptible to corrosion, it remains widely used in industry due to its low cost, availability, and high durability [11]. This situation highlights the need for corrosion inhibitors to extend pipeline service life, among which CrSiN coatings have demonstrated strong corrosion resistance across different environments [12], [13], [14].

To evaluate the performance of CrSiN-coated N80 steel, it is essential to reproduce the fluid transport conditions found in the field under controlled laboratory settings. Hydrodynamic techniques provide a means of assessing the steel's corrosion rate in relation to flow variables such as temperature, velocity, and the size of suspended solids.

In this study, pipeline operating conditions were simulated using a Rotating Cylinder Electrode (RCE), a method widely employed to investigate corrosive and erosive processes in pipelines characterized by turbulent flows. The RCE technique generates a uniform flow with constant velocity and controlled mass transport rates [15], [16].

Simulating the hydrodynamic behavior of such flows requires solving the Navier–Stokes equations, whose complexity necessitates the use of simplification approaches such as turbulence models within computational fluid dynamics (CFD) [17], [18], [19]. Through numerical methods, CFD makes it possible to predict the hydraulic response of different variables [20]. In this study, Reynolds-averaged Navier–Stokes (RANS) turbulence models were used, as they provide a balance between accuracy and computational efficiency [21], [22], making them more practical than Direct Numerical Simulation (DNS) or Large Eddy Simulation (LES) models [23]. RANS models are appropriate in this case, as the system replicates the macroscopic behavior of the flow [21].

Considering the geometry and operation of the RCE, the system produces a curvilinear turbulent flow, for which the realizable k-ε model was selected [24]. This model employs a modified transport equation for the dissipation rate (ε) and defines turbulent viscosity through an alternative formulation compared to the standard k-ε model [25].

By combining experimental techniques with computational modeling, this methodology enables the establishment of service-life criteria and maintenance schedules for pipelines made of N80 steel exposed to aggressive multiphase fluids. These fluids are typically characterized by granular materials of varying sizes and temperatures; conditions commonly found in hydrocarbon extraction industries. The results contribute to ensuring both operational reliability and the safety of industrial and environmental systems.

Methodology

The research was conducted using computational fluid dynamics (CFD) with a realizable k-ε turbulence model implemented in OpenFOAM software. The objective was to simulate the hydrodynamic behavior of a multiphase flow composed of water at different temperatures and granular material. This flow was experimentally reproduced in the laboratory with a Rotating Cylinder Electrode (RCE), providing tools to support preventive maintenance planning for hydraulic installations constructed with N80 steel pipelines coated with CrSiN.

Cylindrical specimens of API 5CT N80 steel pipelines, commonly used for water injection and extraction in hydrocarbon production systems, were coated with CrSiN by Physical Vapor Deposition (PVD) to improve their tribological properties and corrosion resistance [12], [26]. To

The hydraulic system was configured as a multi-fluid system, requiring the definition of phases and interaction elements. The fluid at different temperatures served as the primary phase, sand as the secondary phase, and the steel specimens together with the glass container as the interaction elements.

The hydraulic modeling was based on solving the Navier–Stokes partial differential equations (1) to (3).

$$\rho \frac{Du}{Dt} = -\frac{\partial p}{\partial x} + \mu \left(\frac{\partial^2 u}{\partial x^2} + \frac{\partial^2 u}{\partial y^2} + \frac{\partial^2 u}{\partial z^2} \right) + S_{Mx} \quad (1)$$

$$\rho \frac{Dv}{Dt} = -\frac{\partial p}{\partial y} + \mu \left(\frac{\partial^2 v}{\partial x^2} + \frac{\partial^2 v}{\partial y^2} + \frac{\partial^2 v}{\partial z^2} \right) + S_{My} \quad (2)$$

$$\rho \frac{Dw}{Dt} = -\frac{\partial p}{\partial z} + \mu \left(\frac{\partial^2 w}{\partial x^2} + \frac{\partial^2 w}{\partial y^2} + \frac{\partial^2 w}{\partial z^2} \right) + S_{Mz} \quad (3)$$

For this purpose, the following fundamental aspects of the modeling process were considered:

Spatial Discretization

The process was defined by establishing the mesh for both the boundaries and the polyfluid. In this case, an unstructured triangular mesh was employed due to the system's complexity [29]. The mesh was generated independently for the polyfluid phases (water and sand) as well as for the interaction elements (glass and steel).

Temporal Discretization

This was carried out using an implicit methodology developed for both steady and unsteady flows, considering that the system's experimental hydraulics include a hydrostatic phase followed by a hydrodynamic phase. The latter generates the movement of the multiphase fluid around the specimens under analysis, initially in an accelerated manner until equilibrium is reached at a constant velocity.

Discretization of the equations

This approach enables the algebraic formulation of the differential equations governing the flow, primarily the momentum and continuity equations, whose solution requires sequential development. The SIMPLE algorithm was employed to couple pressure and velocity, allowing the simultaneous resolution of the momentum and continuity equations.

Turbulent flow calculation

Given the strong small-scale fluctuation's characteristic of turbulent flows and the requirement to solve the Navier–Stokes equations, the hydraulic modeling was carried out using a RANS turbulence model. This approach is based on Reynolds decomposition and the time-averaged formulation of the Navier–Stokes equations [30], as outlined below:

Equation 4 represents the mass conservation average:

$$\nabla . \overline{U} = \frac{\partial \bar{u}}{\partial x} + \frac{\partial \bar{v}}{\partial y} + \frac{\partial \bar{w}}{\partial \bar{z}} = 0 \quad (4)$$

Equations 5–7 present the x, y, and z components of the averaged momentum conservation equation:

$$\frac{\partial \bar{u}}{\partial t} + \bar{u}\frac{\partial \bar{u}}{\partial x} + \bar{v}\frac{\partial \bar{u}}{\partial y} + \bar{w}\frac{\partial \bar{u}}{\partial z} = -\frac{1}{\rho}\frac{\partial \bar{p}}{\partial x} + \frac{\mu}{\rho}\nabla^2 \bar{u} + \frac{1}{\rho}\left(\frac{\partial(-\rho\overline{u'u'})}{\partial x} + \frac{\partial(-\rho\overline{u'v'})}{\partial y} + \frac{\partial(-\rho\overline{u'w'})}{\partial z} \right) \quad (5)$$

$$\frac{\partial \bar{v}}{\partial t} + \bar{u}\frac{\partial \bar{v}}{\partial x} + \bar{v}\frac{\partial \bar{v}}{\partial y} + \bar{w}\frac{\partial \bar{v}}{\partial z} = -\frac{1}{\rho}\frac{\partial \bar{p}}{\partial y} + \frac{\mu}{\rho}\nabla^2 \bar{v} + \frac{1}{\rho}\left(\frac{\partial(-\rho\overline{v'u'})}{\partial x} + \frac{\partial(-\rho\overline{v'v'})}{\partial y} + \frac{\partial(-\rho\overline{v'w'})}{\partial z} \right) \quad (6)$$

$$\frac{\partial \bar{w}}{\partial t} + \bar{u}\frac{\partial \bar{u}}{\partial x} + \bar{v}\frac{\partial \bar{u}}{\partial y} + \bar{w}\frac{\partial \bar{u}}{\partial z} = -\frac{1}{\rho}\frac{\partial \bar{p}}{\partial x} + \frac{\mu}{\rho}\nabla^2 \bar{u} + \frac{1}{\rho}\left(\frac{\partial(-\rho\overline{u'u'})}{\partial x} + \frac{\partial(-\rho\overline{u'v'})}{\partial y} + \frac{\partial(-\rho\overline{u'w'})}{\partial z} \right) \quad (7)$$

The application of these equations introduces additional unknowns that must be resolved, necessitating the use of a turbulence model. In this study, the realizable k–ε model was employed, which determines the turbulence length and time scales through two transport equations [31]. This model, a variation of the standard k–ε formulation, is based on the Boussinesq hypothesis and incorporates turbulent viscosity as an additional flow property, defined as follows [32]:

$$\mu_t = \rho C_\mu \frac{k^2}{\varepsilon} \quad (8)$$

In this formulation, equations for k (turbulent kinetic energy) and ε (dissipation rate) are incorporated [31], with a modification to the k equation to prevent normal stresses from becoming negative in flows characterized by high mean strain rates. This condition is ensured by defining CμC_\ muCμ as a variable, which can be calculated using Equation (9) [33]

$$C_\mu = \frac{1}{A_0 + A_S \frac{kU^*}{\varepsilon}} \tag{9}$$

Here, the value of U^+ is defined in Equation (10).

$$U^* = \sqrt{S_{ij}S_{ij} + \widetilde{\Omega_{ij}}\widetilde{\Omega_{ij}}} \tag{10}$$

Equation (11) provides the calculation of the variable $\widetilde{\Omega_{ij}}$

$$\widetilde{\Omega_{ij}} = \Omega_{ij} - 2\varepsilon_{ijk}w_k \tag{11}$$

The values of the constants defined in Equation 9 can be determined as follows:

$A_0 = 4.04$

and $A_S = \sqrt{6}\cos\phi$

being $\phi = \frac{1}{3}cos^{-1}\left(\sqrt{6W}\right)$

y $W = \frac{S_{ij}S_{jk}S_{ki}}{\tilde{S}}$

The application of the realizable k-ε method is well-suited for flows with curvilinear behavior [34], such as that represented in the simulated RCE model. This turbulence model was solved using the finite volume method, which ensures that the equations are addressed under a conservation principle [35]. Finally, the SIMPLE algorithm was selected for pressure–velocity coupling because it adapts effectively to different geometries, is suitable for both incompressible and compressible flows, and avoids excessive computational costs due to its high stability and numerical efficiency [35].

Boundary Conditions of the Model and Standard Wall Functions

The boundary conditions of the model are determined by the simulation setup. The outer boundary corresponds to the external wall of the beaker containing the fluid, composed of two phases: water with NaCl and sand. The inner boundary is defined by the central rotating axis of the equipment, which holds the CrSiN-coated steel samples.

The interaction between the fluid phases and the system boundaries is modeled using wall functions, which are essential for the mathematical simulation of turbulent flow. The boundary conditions, phases, and wall functions are illustrated in Figure 1.

Figure 1. Phases and walls

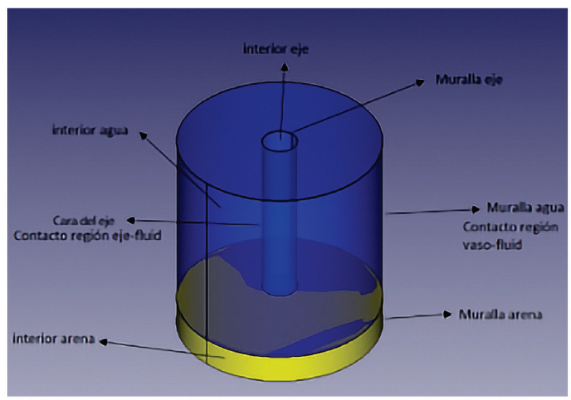

Source: Own elaboration.

The relationship between the experimental reproduction of the fluid's hydrodynamic behavior and its numerical modeling enables the establishment of correlations between the corrosion rate in N80 steel pipes and key process variables, including particulate matter size, flow velocity, and temperature. This correlation is expressed through mathematical models that support the prediction of corrosion rates, providing designers and operators of hydraulic infrastructure with a tool to anticipate and prevent failures caused by corrosion.

Results

The first stage of the hydrodynamic modeling analysis focused on verifying that the simulated fluid velocity matched the velocity at the axis of the RCE, where the steel specimen was located. The results demonstrated that, regardless of the rotational speed of the equipment, the flow temperature, or the average diameter of the solid phase within the flow, the flow lines near the axis exhibited velocities consistent with the rotational speed of the equipment. This validation confirmed the reliability of the modeling, enabling further analysis of the modeled mass volume on the specimen and the velocity of the particulate material in its vicinity.

Once the fluid velocity was established, the modeling facilitated the characterization of the particulate phase under different fluid configurations (axis rotational speed, fluid temperature, and particle size). First, the trajectories of the suspended particles within the fluid were determined (see Figure 2). Next, the velocity of these particles and the mass volume in contact with the analyzed N80 steel were quantified.

Figure 2. Simulation of the solid phase of the flow (V: 2000 rpm, Diameter: 0.05 mm, and Temperature: 25°C)

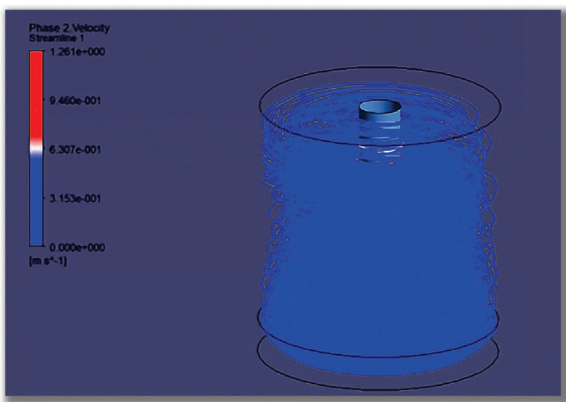

Source: Own elaboration.

Corrosion Rate

The measurement of this variable was carried out using an RCE, employing a $3^2 \times 2^1$ parametric model. This process required N80 steel samples coated with a CrSiN layer, resulting in a total of 18 tests (with corresponding replicas). To evaluate the effectiveness of the coating, an equal number of uncoated N80 steel samples were also analyzed to establish the baseline corrosion rate of the steel.

The RCE measurements demonstrated that applying a CrSiN layer to N80 steel is highly effective in reducing the corrosion rate, achieving a reduction of two orders of magnitude compared to uncoated N80 steel. Additionally, the flow rotation speed was found to directly influence the corrosion rate, particularly in fluids containing particles of 0.1 and 0.15 mm. This effect is associated with the impact force on the specimens, which is determined by both the size of the particulate matter and its kinetic energy upon reaching the steel surface.

The corrosion rate of steel increases with the diameter of the particulate matter; however, for 0.15 mm particles, the rate decreases. This reduction may be attributed to the inability of the flow's drag force to transport heavier particles efficiently. Furthermore, as the temperature of the multiphase flow rises, the corrosion rate also increases, a behavior linked to the acceleration of oxidation reactions.

To further identify the mechanisms contributing to corrosion in N80 steel, each sample exposed to the aggressive flow in the RCE was examined using SEM imaging. The analyses revealed irregularities and defects in the CrSiN coating, including scratch marks, impact sites, and localized areas of material detachment showing evidence of corrosion. The presence of silicon oxides, originating from the solid particles in the multiphase fluid, was also detected. These findings confirm that the wear of the coating is primarily caused by the abrasive action of sand particles.

Particulate Material Velocity

The conducted simulations indicate that, regardless of flow velocity, temperature, or mean particle diameter, the average velocity of suspended particles remains lower than that of the flow. This phenomenon occurs consistently, with minimal changes in particle velocity as fluid temperature increases. Although temperature variations alter the fluid's physical properties (such as density and viscosity),

the observed behavior suggests that, despite changes in electrolyte characteristics, the impact of the flow's drag force on the solid phase is primarily influenced by the solid phase's weight and flow velocity.

As previously mentioned, the drag force exerted by the fluid is directly related to rotational speed and the specific weight of the solid phase, affecting the velocity of the particulate material. Thus, in fluids subjected to speeds of 250 and 1250 RPM, an increase in particle diameter and weight results in a velocity decrease, with this effect being more pronounced for larger particles (0.15 mm). Likewise, at 2000 RPM, while the same trend persists, the increased drag force prevents the velocity of larger particles from decreasing as significantly as in the previous cases.

This behavior is explained by the increase in the specific weight of the materials, which requires greater force for transport at higher speeds. The described trend is illustrated in Figure 4.

There is a direct relationship between the simulated solid-phase velocity values and the observed steel corrosion rates. This relationship arises from the deterioration caused by the impact of solid particles on the CrSiN coating, which exposes the underlying steel and compromises its corrosion resistance.

The results indicate that, for a given particle size, an increase in flow velocity leads to higher corrosion rates. This behavior is driven by the greater kinetic energy exerted on the coating by both the fluid and the solid phase. Across all flow velocities, a consistent trend was observed: corrosion rates increase when particle size rises from 0.05 mm to 0.1 mm but decrease for larger particles (0.15 mm). This reduction is more pronounced at lower flow velocities, a phenomenon linked to the hydrodynamic response of the multiphase flow, as reflected by the velocity of the solid phase. The behavior is consistent with the inability of low-velocity flows to effectively transport heavier particles [4].

The relationship between corrosion rate, flow velocity, and particle diameter is illustrated in Figure 5.

Figure 3. Velocity of the solid phase as a function of its size

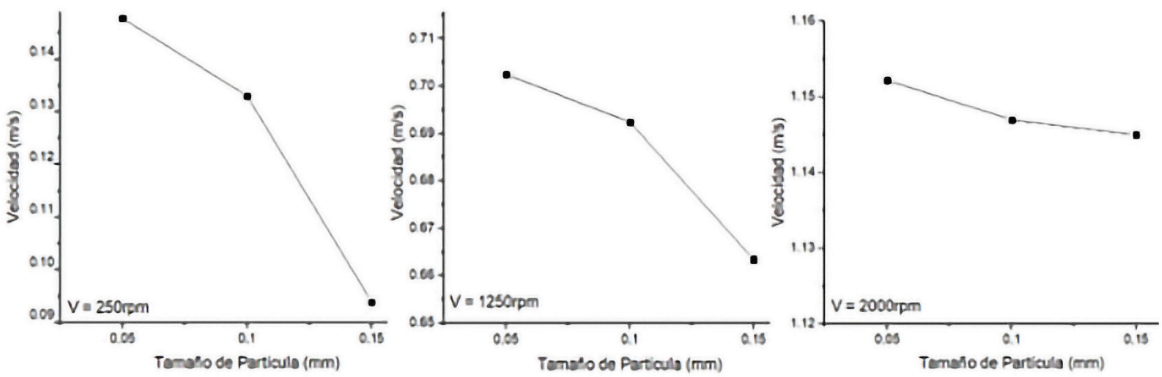

Source: Own elaboration.

Figure 4. Corrosion rate in relation to flow velocity and particle diameter

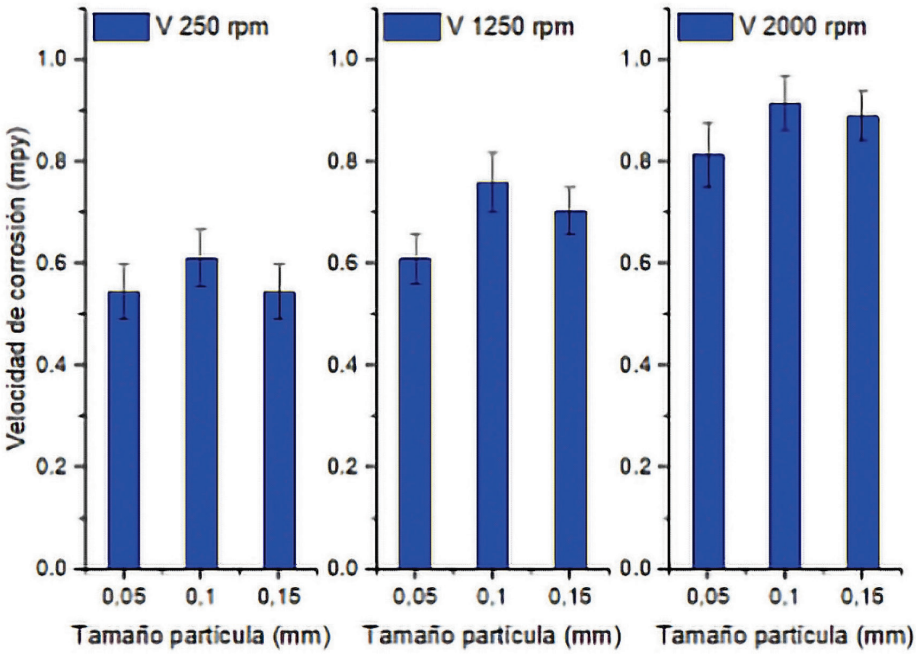

Source: Own elaboration.

Fractional Volume

In this study, the fluid is characterized as a multiphase mixture that includes particulate material. The determination of the fractional volume requires analyzing, under different configurations of fluid velocity, temperature, and particle size, the proportion of the solid phase deposited on the surfaces of the N80 steel specimens tested in the ECR.

The modeling of the fractional volume shows that, similar to the behavior observed for silica sand velocity, at a constant flow velocity, an increase in particle diameter leads to a reduction in the proportion of solid particles near the surface of the tested specimens. This finding reinforces the observation that the fluid lacks the capacity to effectively transport heavier particles to the coated steel surfaces.

Figure 5. Mass volume as a function of velocity

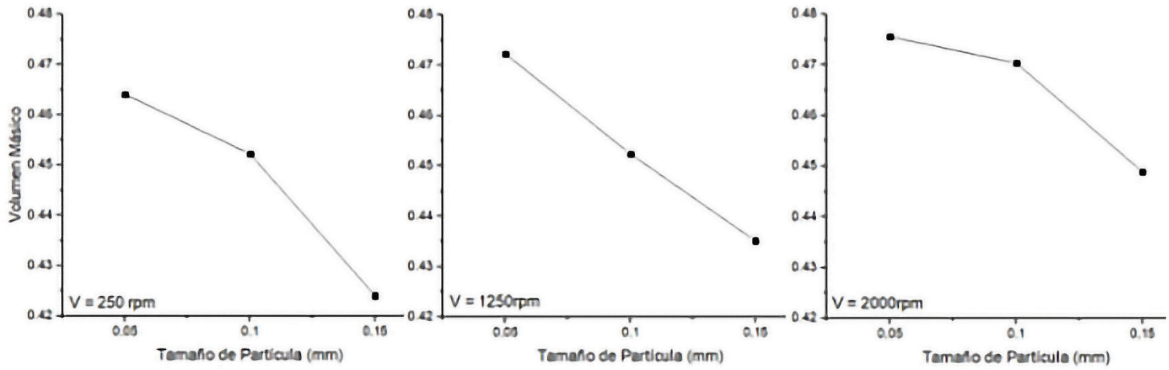

Source: Own elaboration.

The volume of solids reaching the walls of the analyzed steel is influenced by temperature increases under low-velocity flow conditions. For the same particle size, higher temperatures result in a reduced amount of particulate material deposited on the test specimen. This behavior is attributed to the decrease in fluid density caused by temperature rise.

Conversely, at medium and high rotational velocities, this variable becomes less significant. Although fluid density decreases with increasing temperature, the higher velocities provide sufficient energy to enhance the transport of suspended material. This effect highlights the predominant role of flow velocity in controlling particulate transport in moving fluids.

Consistent with the behavior observed for particulate velocity, the fractional volume reaching the specimen walls is also affected by particle weight. At constant fluid velocity, the proportion of solids decreases as particle size increases. The described trend is illustrated in Figure 6.

Figure 6. Mass volume in relation to fluid temperature

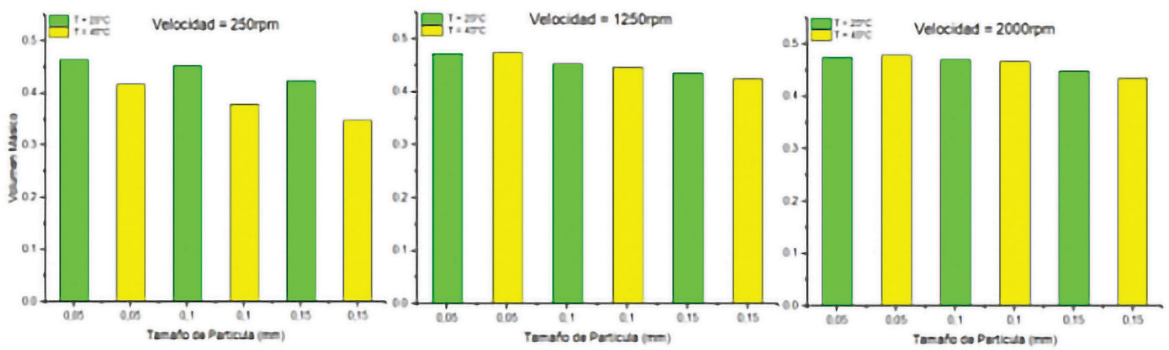

Source: Authors.

Regression Models

A mathematical expression was developed to determine the corrosion rate (Vc) of N80 steel coated with a CrSiN layer, based on hydrodynamic variables and the characteristics of the multiphase fluid. The first approach considered the solid phase velocity within the sample (Vp) as a hydrodynamic response parameter, together with fluid properties such as temperature (T) and silica sand particle size (t). These three regressors were used to construct a multivariable linear regression model. The resulting mathematical expression is presented as follows:

$$V_C = -0.5699 + 0.5179 * V_p + 1.1341 * t + 0.0331 * T \quad (16)$$

To establish the relationship between the experimental corrosion rate measurements obtained from the ECR and the results derived from the regression models, the cross-correlation coefficient and the coefficient of determination (R^2) were calculated, yielding values of 0.94 and 0.88, respectively. These results confirm both the accuracy and the reliability of the proposed mathematical expression.

In pursuit of achieving stronger correlations between the experimental data and the outputs of the mathematical models, the fractional volume (VF), defined for each multiphase fluid configuration through hydrodynamic simulation, was incorporated. A linear regression model with four regressors was thus developed, resulting in the following expression.

$$V_c = -2.599 + 0.314 * V_p + 2.963 * t + 0.038 * T + 4.064 * VF \quad (17)$$

For this model, a cross-correlation coefficient of 0.95 and an R^2 value of 0.90 were obtained. These results indicate that incorporating the fractional volume into the multiple linear regression models enhances the reliability of the mathematical expression derived from the fluid configuration and hydrodynamic results. The two derived expressions are subject to the following applicability limits:

- Velocity of particulate material: 0.138 – 1.152 m/s
- Electrolyte temperature: 25 – 45°C
- Particle size: 0.05 – 0.15mm

These mathematical expressions can serve as a tool for design engineers and operating personnel to anticipate the corrosion response of N80 steel piping systems exposed to hydrodynamic conditions with aggressive flows. This approach is particularly valuable for risk management in hydrocarbon extraction facilities, as it integrates pipeline operating condition simulations with computational system modeling

Conclusions

The results of the hydrodynamic modeling indicate that the simulated velocity of fluid particles near the steel specimen corresponds to the values measured experimentally in the ECR. Furthermore, the velocity of the silica sand and the fractional volume of material reaching the specimen were quantified. Based on these findings, it was established that the corrosion rate is directly influenced by fluid velocity and sand particle size (for diameters of 0.05 mm and 0.1 mm). However, this relationship does not hold for larger particles, where a reduction in the fluid's transport capacity and a decrease in the particles' impact energy on the coating were observed.

Mathematical expressions were derived using regression models with three and four predictors to estimate the corrosion rate, considering experimental system variables (fluid temperature and sand particle diameter) and simulated hydrodynamic variables (particulate velocity and fractional volume). The analysis revealed that the four-predictor model achieved higher correlation coefficients between measured and simulated data, indicating that incorporating fractional volume improves the prediction of the corrosion rate in CrSiN-coated N80 steel.

References

[1] H. S. Klapper, D. Laverde, and C. Vasquez, "Evaluation of the corrosion of UNS G10200 steel in aerated brines under hydrodynamic conditions," *Corros Sci*, vol. 50, no. 9, pp. 2718–2723, Sep. 2008, DOI: 10.1016/J.CORSCI.2008.06.022.

[2] N. C. Raguá, M. J. Vera, D. Y. Peña B, and en Corrosión, "Erosión - corrosión de un acero aisi sae 1020 en un sistema salmuera-co2- arena," *Scientia et Technica*, vol. 1, no. 35, pp. 213–218, Jan. 2007, Accessed: May 20, 2024. [Online]. Available: https://revistas.utp.edu.co/index.php/revistaciencia/article/view/5413

[3] Y. Yang and Y. F. Cheng, "Parametric effects on the erosion–corrosion rate and mechanism of carbon steel pipes in oil sands slurry," *Wear*, vol. Complete, no. 276–277, pp. 141–148, Feb. 2012, DOI: 10.1016/J.WEAR.2011.12.010.

[4] S. A. Bradford, "Corrosion control," p. 553, 2001.

[5] Pierre R. Roberge, *Handbook of Corrosion Enginee*. 1999. Accessed: May 21, 2024. [Online]. Available: https://dl.icdst.org/pdfs/files/441d337b7410198db6d96e61a6716302.pdf

[6] S. Pardo-Díaz, D. Rojas-Tapias, F. Roldan, P. Brandão, and E. Almansa-Manrique, "Biodegradación de fenol en aguas tratadas de la industria petrolera para re-uso en cultivos agrícolas," *Rev Biol Trop*, vol. 65, no. 2, pp. 685–700, 2017, DOI: 10.15517/RBT.V65I2.23992.

[7] M. Varkas, E. Papamichos, and A. N. Berntsen, "Experimental study of volumetric sand production with gas flow," *Geoenergy Science and Engineering*, vol. 234, p. 212610, Mar. 2024, DOI: 10.1016/J.GEOEN.2023.212610.

[8] G. Mubarak, C. Verma, I. Barsoum, A. Alfantazi, and K. Y. Rhee, "Internal corrosion in oil and gas wells during casings and tubing: Challenges and opportunities of corrosion inhibitors," *J Taiwan Inst Chem Eng*, vol. 150, Sep. 2023, DOI: 10.1016/J.JTICE.2023.105027.

[9] F. Ge, T. Shao, C. Jia, P. Li, and F. Huang, "Tribological behaviors of a magnetron sputtered CrSiN coating under ambient air and wet environments," *Surf Coat Technol*, vol. 332, pp. 304–311, Dec. 2017, DOI: 10.1016/J.SURFCOAT.2017.05.093.

[10] C. Alberto da Silva, D. Filho, T. Pimentel, and Z. Panossian, "Analysis of crude oil effect for CO2 corrosion of carbon steel - A rotating cylinder electrode approach," *Geoenergy Science and Engineering*, vol. 229, Oct. 2023, DOI: 10.1016/J.GEOEN.2023.212085.

[11] A. Ait Mansour *et al.*, "Investigating corrosion failure in N80 carbon Steel: Experimental and theoretical insights into isonicotinohydrazide derivatives as inhibitors in acidic conditions," *Inorg Chem Commun*, vol. 161, Mar. 2024, DOI: 10.1016/J.INOCHE.2023.112007.

[12] H. Chen, Y. Ye, C. Wang, X. Ma, H. Wang, and W. Liu, "Understanding the corrosion and tribological behaviors of CrSiN coatings with various Si contents in HCl solution," *Tribol Int*, vol. 131, pp. 530–540, Mar. 2019, DOI: 10.1016/J.TRIBOINT.2018.11.018.

[13] Y. Fu, F. Zhou, and M. Zhang, "The enhancement of individual friction and corrosion properties of CrSiN coatings by Mo doping in seawater," *Surf Coat Technol*, vol. 432, Feb. 2022, DOI: 10.1016/J.SURFCOAT.2021.128069.

[14] L. Shan, Y. R. Zhang, Y. X. Wang, J. L. Li, X. Jiang, and J. M. Chen, "Corrosion and wear behaviors of PVD CrN and CrSiN coatings in seawater," *Transactions of Nonferrous Metals Society of China (English Edition)*, vol. 26, no. 1, pp. 175–184, Jan. 2016, DOI: 10.1016/S1003-6326(16)64104-3.

[15] M. M. Stack, J. S. James, and Q. Lu, "Erosion-corrosion of chromium steel in a rotating cylinder electrode system: Some comments on particle size effects," *Wear*, vol. 256, no. 5, pp. 557–564, Mar. 2004, DOI: 10.1016/S0043-1648(03)00565-9.

[16] F. C. Walsh, G. Kear, A. H. Nahlé, J. A. Wharton, and L. F. Arenas, "The rotating cylinder electrode for studies of corrosion engineering and protection of metals—An illustrated review," *Corros Sci*, vol. 123, pp. 1–20, Jul. 2017, DOI: 10.1016/J.CORSCI.2017.03.024.

[17] D. Richard, M. Tom, J. Jang, S. Yun, P. D. Christofides, and C. G. Morales-Guio, "Quantifying transport and electrocatalytic reaction processes in a gastight rotating cylinder electrode reactor via integration of Computational Fluid Dynamics modeling and experiments," *Electrochim Acta*, vol. 440, Feb. 2023, DOI: 10.1016/J.ELECTACTA.2022.141698.

[18] M. W. Lohry and L. Martinelli, "On the development, verification, and validation of a discontinuous Galerkin solver for the Navier-Stokes equations," *Comput Fluids*, vol. 229, p. 104990, Oct. 2021, DOI: 10.1016/J.COMPFLUID.2021.104990.

[19] H. Chen and M. Hall, "CFD simulation of floating body motion with mooring dynamics: Coupling MoorDyn with OpenFOAM," *Applied Ocean Research*, vol. 124, Jul. 2022, DOI: 10.1016/J.APOR.2022.103210.

[20] A. Villamizar Hernández, "Aplicación de un modelo turbulento bidimensional para la simulación de flujo a superficie libre en un canal horizontal," 2014, Accessed: May 21, 2024. [Online]. Available: https://repositorio.unal.edu.co/handle/unal/53225

[21] M. Liu, C. Jiang, B. C. Khoo, H. Zhu, and G. Gao, "A cell-based smoothed finite element model for the analysis of turbulent flow using realizable k-ε model and mixed meshes," *J Comput Phys*, vol. 501, Mar. 2024, DOI: 10.1016/J.JCP.2024.112783.

[22] Y. Liao, H. Hessenkemper, D. Lucas, and T. Ma, "Revisiting RANS turbulence modelling for bubble-induced turbulence: Effects of surfactants," *Chemical Engineering Research and Design*, vol. 205, pp. 510–516, May 2024, DOI: 10.1016/J.CHERD.2024.04.026.

[23] L. D. Mendoza, L. E. Vera, and L. E. Vera, "Study of different turbulence models to obtain the curves characteristics of a naca profile 2415 through the three-dimensional simulation of fluid flows," *BISTUA REVISTA DE LA FACULTAD DE CIENCIAS BASICAS*, vol. 0, no. 0, pp. 43–51, Nov. 2019, DOI: 10.24054/01204211.V3.N3.2019.3563.

[24] F. Liu, T. Lu, K. Li, C. Xie, and H. Zhao, "Computational fluid dynamics study on the effect of stirring parameters on solid–liquid suspension in the slurry electrolysis square tank," *Advanced Powder Technology*, vol. 34, no. 5, p. 104016, May 2023, DOI: 10.1016/J.APT.2023.104016.

[25] M. Kadivar, D. Tormey, and G. McGranaghan, "A comparison of RANS models used for CFD prediction of turbulent flow and heat transfer in rough and smooth channels," *International Journal of Thermofluids*, vol. 20, p. 100399, Nov. 2023, DOI: 10.1016/J.IJFT.2023.100399.

[26] T. Shao *et al.*, "Microstructural effect on the tribo-corrosion behaviors of magnetron sputtered CrSiN coatings," *Wear*, vol. 416–417, pp. 44–53, Dec. 2018, DOI: 10.1016/J.WEAR.2018.10.001.

[27] J. Z. Yi, H. X. Hu, Z. B. Wang, and Y. G. Zheng, "On the critical flow velocity for erosion-corrosion of Ni-based alloys in a saline-sand solution," *Wear*, vol. 458–459, Oct. 2020, DOI: 10.1016/J.WEAR.2020.203417.

[28] S. Kim, K. Choi, and J. Jung, "Improvement of CFD code for two-phase flow with boiling and natural convection for evaluation of core-catcher cooling performance in OpenFOAM," *Nuclear Engineering and Design*, vol. 408, p. 112316, Jul. 2023, DOI: 10.1016/J.NUCENGDES.2023.112316.

[29] A. Lozano Durán, "Apuntes sobre Dinámica de Fluidos Computacional," *GNU Free Documentation License*, 2015.

[30] A. S. Cato, P. S. Volpiani, V. Mons, O. Marquet, D. Sipp, and P. Stefanin Volpiani, "Journal Pre-proof Comparison of different data-assimilation approaches to augment RANS turbulence models Comparison of different data-assimilation approaches to augment RANS turbulence models," 2023, DOI: 10.1016/j.compfluid.2023.106054.

[31] M. Aydogdu, "Analysis of the effect of rigid vegetation patches on the hydraulics of an open channel flow with Realizable k-ε and Reynolds stress turbulence models," *Flow Measurement and Instrumentation*, vol. 94, p. 102477, Dec. 2023, DOI: 10.1016/J.FLOWMEASINST.2023.102477.

[32] J. A. Yáñez-Varela, I. González-Neria, A. Alonzo-García, G. Rivadeneyra-Romero, and S. A. Martínez-Delgadillo, "Numerical analysis of the hydrodynamics induced by rotating ring electrode using κ-ε models," *Chemical Engineering and Processing - Process Intensification*, vol. 158, Dec. 2020, DOI: 10.1016/J.CEP.2020.108203.

[33] H. , and M. W. Versteeg, "Introducción a la dinámica de fluidos computacional - Recursos Educativos Abiertos." Accessed: May 21, 2024. [Online]. Available: https://blogs.ugto.mx/rea/clase-digital-1-introduccion-a-la-dinamica-de-fluidos-computacional/

[34] dos Santos, E. D. dos Santos, C. M. Xavier, and A. P. Petry, "Estudio Numérico de Flujos Turbulentos Isotérmicos en Canales y Flujos Laminares con Convección Mixta en Cavidades," *Información tecnológica*, vol. 22, no. 1, pp. 71–82, 2011, DOI: 10.4067/S0718-07642011000100010.

[35] J. Xamán and M. Gijón-Rivera, "Dinámica de fluidos computacional para ingenieros," p. 418, 2013.